Many-body localization and transition by density matrix renormalization group and exact diagonalization studies

S. P. Lim and D. N. Sheng

Phys. Rev. B **94**, 045111 — Published 13 July 2016

DOI: 10.1103/PhysRevB.94.045111

Nature of Many-Body Localization and Transition by Density Matrix Renormaliztion Group and Exact Diagonalization Studies

S. P. Lim and D. N. Sheng
Department of Physics and Astronomy, California State University, Northridge, California 91330, USA

A many-body localized (MBL) state is a new state of matter emerging in a disordered interacting system at high energy densities through a disorder driven dynamic phase transition. The nature of the phase transition and the evolution of the MBL phase near the transition are the focus of intense theoretical studies with open issues in the field. We develop an entanglement density matrix renormalization group (En-DMRG) algorithm to accurately target highly excited states for MBL systems. By studying the one dimensional Heisenberg spin chain in a random field, we demonstrate the accuracy of the method in obtaining energy eigenstates and the corresponding statistical results of quantum states in the MBL phase. Based on large system simulations by En-DMRG for excited states, we demonstrate some interesting features in the entanglement entropy distribution function, which is characterized by two peaks; one at zero and another one at the quantized entropy $S = ln2$ with an exponential decay tail on the $S > ln2$ side. Combining En-DMRG with exact diagonalization simulations, we demonstrate that the transition from the MBL phase to the delocalized ergodic phase is driven by rare events where the locally entangled spin pairs develop power-law correlations. The corresponding phase diagram contains an intermediate or cross over regime, which has power-law spin-z correlations resulting from contributions of the rare events. We discuss the physical picture for the numerical observations in this regime, where various distribution functions are distinctly different from results deep in the ergodic and MBL phases for finite-size systems. Our results may provide new insights for understanding the phase transition in such systems.

PACS numbers: 73.40.Hm, 71.30.+h, 73.20.Jc

I. INTRODUCTION

Understanding the effects of interaction on Anderson localization[1–6] has led to a rapidly expanding field, where a new correlated state of matter, a many-body localized (MBL) phase emerges[7–13]. Many remarkable properties of an MBL phase has been established[7–51] based on extensive theoretical studies. For disordered interacting systems, a random disorder can drive a dynamic phase transition[7, 12, 52] from a delocalized state to an MBL phase, where all energy eigenstates become localized. Protected by the localization, an MBL phase is non-ergodic and can not thermalize[14, 53, 54], which also challenges the fundamental "eigenstate thermalization hypothesis" (ETH) for quantum statistical physics[55]. The energy eigenstate in an MBL phase has entanglement entropy satisfying an area law[7, 23, 28, 29] scaling in contrast to the volume law scaling expected for an ergodic delocalized state. The MBL phase behaves like integrable systems, respecting extensive numbers of local conservation laws [9, 20, 21, 56] with the emergence of the localized-bits (l-bit) representing these conserved local degrees of freedom. Interestingly, exotic topological states usually present at low temperature, can survive to infinite temperature in an MBL environment[22, 28, 32, 57–61], which greatly enhances the possibility of their applications in future topological quantum computing. There are also growing experimental activities observing and probing the nature of the MBL phase and phase transition in cold atom systems [15–18, 62–64].

So far, theoretical understanding of the dynamic phase transition is still at the beginning stage[11–13, 15, 18, 19, 23, 26–31, 33–39, 45, 51, 65–67]. Larger sizes (with up to $N = 22$ spins) numerical exact diagonalization (ED) studies[66] of the 1D Heisenberg chain in a random field have demonstrated a continuous phase transition between a delocalized ergodic phase to an MBL phase based on extensive finite-size scaling analysis of different physical quantities including the entanglement entropy and the energy level statistics. The numerical linked cluster expansion calculations suggest a higher critical disorder strength for entering the MBL phase[68] than that obtained by ED studies[66]. Theoretical[19] and numerical studies of the low frequency conductivity[24, 25] and energy spectra statistics[45] have suggested that there is an intermediate regime with sub-diffusive conductivity and (or) semi-Poisson level statistics between the ergodic and MBL phases. A consistent picture for understanding the dynamic phase transition and transport properties[69, 70] in such a system is still absent. One of the difficulties is the presence of rare Griffiths regions[19, 25, 52] which may have singular contributions in driving a phase transition. However, so far there is still limited quantitative understanding about their effects.

To make progress, it is highly desirable to study much larger systems[71] and to establish the nature of the MBL phase in the thermodynamic limit, which are great challenges for such a correlated system at finite energy density. The MBL phase has low entanglement similar to groundstates of low dimensional systems, which has stimulated a lot of recent effort in developing the density matrix renormalization group (DMRG)[72] or tensor network based new algorithms for studying such systems[65, 73–78]. Exciting progress has been made including developing modified DMRG methods to target eigenstates [76–78] in the high energy density region. One of the main issues that remains to be addressed is if it is possible to use the DMRG method to unbiasedly obtain different excited states with intrinsically fluctuating entanglement

entropy for large systems. Only when the DMRG method for excited states can overcome the tendency of picking minimum entangled states[79] among all excited states at a finite energy density, will it establish itself as a powerful tool for studying challenging and fundamental issues in quantum statistics emerging with the MBL phase.

In this article, we report developing a new entanglement DMRG (En-DMRG) algorithm to meet this challenge. The En-DMRG will randomly select and target the entanglement pattern of the highly excited states in an MBL system. By studying the one dimensional Heisenberg spin chain in a random field, we demonstrate the high accuracy of the method in obtaining excited states and reproducing statistical features of the system in comparison with ED results. Based on large system simulations with up to $N = 72$ spins by En-DMRG, we first show that a spin-flip process and the associated spin-entangled pairs have a finite and system-size independent probability density in the MBL phase. We also obtain the characteristic probability density distribution function for the entaglement entropy, which has a continuous spectrum with a sharp peak at the quantized entropy value $S = ln2$ and an exponential decay tail on the $S > ln2$ side for the MBL phase in agreement with the earlier observations based on smaller system studies for different MBL systems[28, 51, 77]. Combining En-DMRG with ED simulations, we study the driving force of the dynamic phase transition from the MBL phase to the ergodic phase. We find that spins first become power-law entangled, which leads to a strong enhancement in the probability distribution function of the entanglement entropy (fluctuation of half system magnetization) on the larger entropy (fluctuation) side. We also identify an intermediate regime where the rare events contribute significantly to the average of the spin correlations. Our results may provide new insights for understanding the rich physics of the MBL phase and the exotic dynamic phase transition in such systems.

II. EN-DMRG METHOD FOR HIGHLY EXCITED STATES

The standard DMRG[72] created by White is an unbiased and controlled method for obtaining the ground state or a few low energy excited states of interacting systems. The true power of the method is in its way of constructing the Hilbert space (HS) by using the eigenstates of the reduced density matrix. To target excited states in an MBL system, we develop an En-DMRG method based on the standard DMRG with modified initial sweeping process to optimally construct larger HS for these states. During this process, we use a varying bond dimension to allow a natural development of an entanglement structure for the quantum state, which leads to a rapid convergence of the entanglement entropy. Here, we outline the basic steps of the En-DMRG. (i) We start from the standard DMRG[72] using the "infinite" process. (ii) Once our system reaches the required system size with N spins, we start the sweeping process to build the HS with a varying bond dimension. The bond dimension will be adjusted according to the truncation error which can be set to be a small value less than 10^{-8}. (iii) We use the Lanczos method to obtain the lowest six energy eigenstates of the squared Hamiltonian $H_2 = (H-E_t)^2$ (E_t is the target energy). We usually keep the lowest energy eigenstate for the reduced density matrix[72] unless specified below for the purpose of optimization. (iv) The En-DMRG process takes more sweeps to reach convergence compared to the ground state DMRG. One can enhance the performance of the En-DMRG by setting a lower accuracy for the Lanczos diagonalization in the initial few sweeps to speed up the calculations, while one can increase the accuracy to the order of 10^{-12} gradually to obtain accurate wavefunction until the targeted state is converged.

Now we discuss the possible optimization for the En-DMRG process. We start from targeting one state near E_t. During the sweeping process, we define the wavefunction overlap $O = | < \Psi_{l-1}|\Psi_l > |$ between the wavefunction $|\Psi_l >$ of the current l step of the En-DMRG sweeping and the wavefunction at the previous step $|\Psi_{l-1} >$ to monitor the evolution of the wavefunction. Sometimes O becomes much smaller than 1 indicating the difficulty of convergerence in the En-DMRG for excited state without proper optimization. In that case, besides keeping the ground state of H_2, we keep additional one or two states among the lowest six energy eigenstates of H_2 according to their overlaps with the previous ground state $|\Psi_{l-1} >$. We also increase the bond dimension m to enlarge the HS at the same time. The idea of optimizing for the overlap of the wave-function at two consecutive steps during the sweeping is similar to the DMRG-X[76, 77] method proposed by Khemani et al. Alternatively, one can also just always keep the lowest energy eigenstate of H_2 and graduatelly increase the bond dimension and Lanczos accuracy to improve the overlap O. After a few sweeps (around $2 - 20$ depending on the disorder configuration and h), we find that the overlap O usually is stablized to be near 1 with a small error controlled by the truncation error of the En-DMRG. This signals that we have built a proper HS for the excited state with its entanglement pattern established and now only a small number of the Lanczos iterations is required to find an accurate eigenstate using the wavefunction transformation following the standard DMRG[72].

We also note that the En-DMRG method is simply using the Lanczos method to find eigenstates of the square Hamiltonian H_2. The method works here because in the DMRG approach, we are using the reduced density matrix eigenstates as the input for building the HS. The eigenstates with energies close to the target state can be projected out because they are locally distinct (different) from the target state for an MBL system as established by the ED study of Luitz et al[66]. By projecting out nearby energy eigenstates, one is dealing with an effective system with larger spectrum gap, which allows the En-DMRG to find the high energy eigenstate accurately. The aim of our work is to establish the accuracy of the En-DMRG for excited states and their quantum statistics for *large* MBL systems as we will demonstrate below, while the latter has not been addressed

so far. In combining with the ED simulation on the smaller disorder side (where the DMRG method is not applicable because of the volume entanglement and the wavefunction similarity for nearby eigenstates) for the delocalized phase, we will explore the nature of the MBL phase and its transition.

We study the Heisenberg spin-1/2 chain with the following Hamiltonian:

$$H = \sum_{i=1}^{N-1} \vec{S}_i \cdot \vec{S}_{i+1} - \sum_i h_i S_i^z,$$

where the nearest neighbor coupling $J = 1$ sets the energy scale and we use open boundary for a better convergence in DMRG. The $h_i's$ are the random magnetic field couplings, which distribute uniformly in the interval $(-h, h)$ with h as the strength of random fields. The ED studies using system sizes $N = 12 - 22$ established an MBL phase at $h \gtrsim 3.5$[66]. The En-DMRG allows us to study larger systems up to $N = 72$ spins, which substantially enlarges the size-range of the finite-size scaling analysis for the MBL phase. All results are obtained near the center of the energy spectrum.

To demonstrate the convergence of the process for our larger system calculation with $N = 72$ at $h = 8$, we show the evolution of the logarithm of the energy variances $\sigma^2 = \langle H^2 \rangle - \langle H \rangle^2$ in Fig. 1a for each sweep of the En-DMRG process, which usually is proportional to the energy error of the state obtained by the En-DMRG. Eight different En-DMRG targeting runs are illustrated in Fig. 1 from one

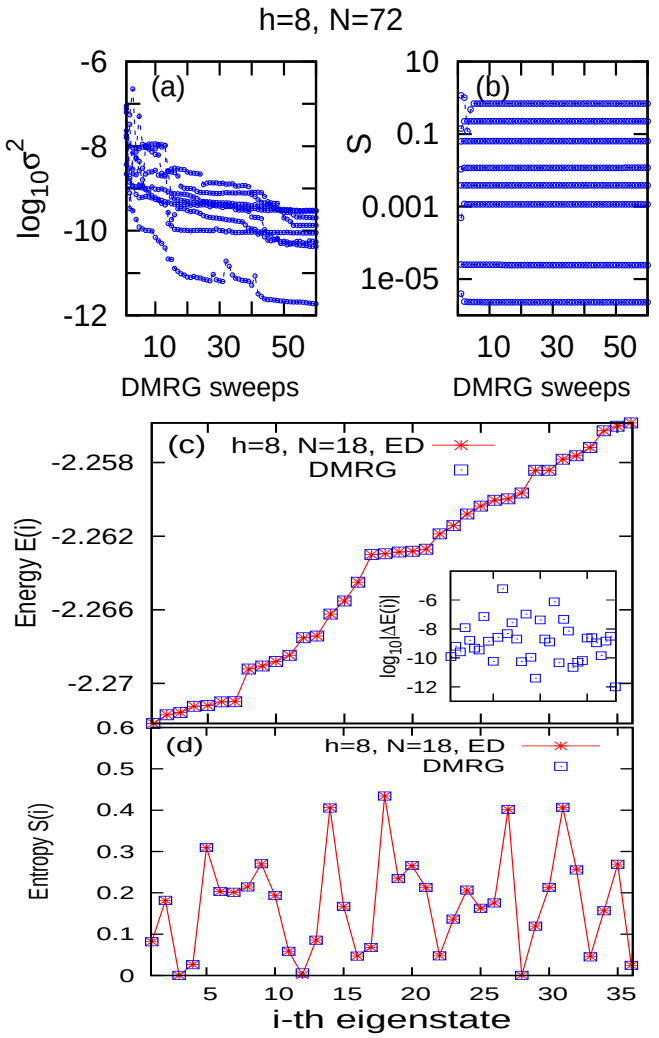

FIG. 1: (Color online) (a) The logarithm of the energy variance σ^2 as a function of the number of En-DMRG sweeps for 8 randomly selected En-DMRG processes for system size $N = 72$ and $h = 8$ targeting the state at the middle of the energy spectrum. (b) The entropy S evolution for the same processes. (c) For smaller system $N = 18$ at $h = 8$, we show the energy eigen values for $i - th$ eigenstate found in the energy interval $(-2.272, -2.257)$ near the energy spectrum center, where an excellent agreement between the En-DMRG and ED results is found. The absolute energy difference $|\Delta E|$ between En-DMRG and ED eigenstates are shown in the inset of (c), which typically is around 10^{-9}. (d) For all 36 states we found in (c), we demonstrate their one to one correspondence for entanglement entropy S between ED and En-DMRG results.

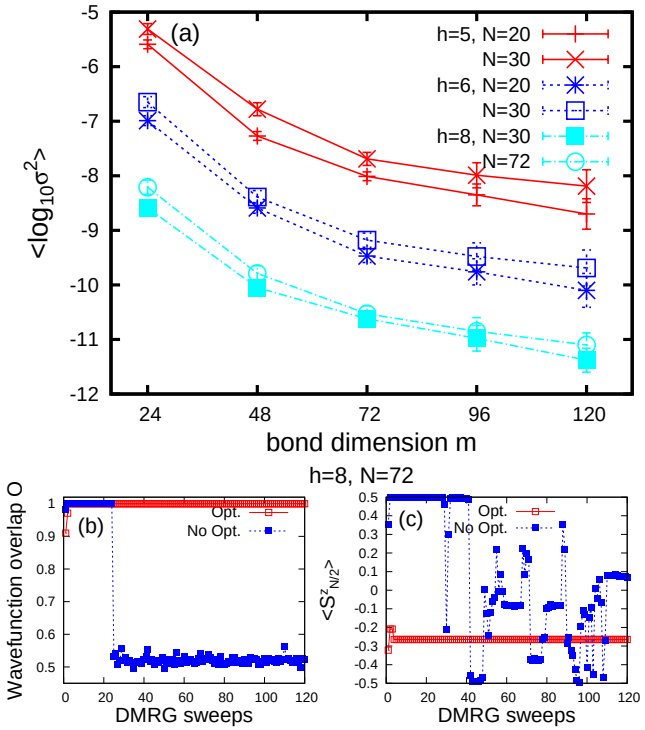

FIG. 2: (Color online) (a) The logarithm of the energy variance σ^2 as a function of the number of the maximum bond dimension m used in En-DMRG averaged over 10000 configurations for bond dimesnions $m \leq 48$ and more than 1000 configurations for larger m. (b) The typical wavefunction overlap O between the current lowest energy state (for H_2) and the state at the previous step for the En-DMRG with and without the proper optimization for each DMRG sweep measured when the En-DMRG sweeps to the middle of the system. (c) The expectation value of spin-z $< S^z_{N/2} >$ during the En-DMRG sweeping for the cases described in (b).

random disorder configuration, and we use an initial bond dimension $M = 24$ and vary it up to $M = 72$ during the sweeping process. We find that the σ^2 starts from around 10^{-8} for the first a few sweeps and drops to around 10^{-10} within 60 sweeps, where we complete the En-DMRG process to find an energy eigenstate near the target energy $E_t = -1.1$. The corresponding bipartite entanglement entropies are shown in Fig. 1b, where amazingly we find that entropy S is well converged after a few initial sweeps. As also demonstrated here, the eigenstates we obtain have a reasonable variance of S values reflecting different levels of entanglement of the targeted eigenstates.

To benchmark our results at a smaller size $N = 18$ and $h = 8$, we show the comparison between eigen energies obtained using ED (red star) and En-DMRG (blue box) with a varying bond dimension around $M = 16 \sim 48$, where an excellent agreement is demonstrated for all energy eigenstates in the energy interval $(-2.272, -2.232)$ near the energy spectrum center for one disorder configuration. The absolute energy difference $|\Delta E|$ between En-DMRG and ED eigenstates are shown in the inset of the Fig. 1c, which typically is around 10^{-9}. In En-DMRG targeting we run about 1000 times with slightly different targeting energy E_t each time. Some states are found more frequently than other states. In Fig. 1d, we show their one to one correspondence for entanglement entropy S from ED and En-DMRG calculations. Very interestingly, we also find that entropies intrinsically fluctuate for these states with very close energies, and En-DMRG can capture them all precisely. However, due to the unequal appearance of the different eigenstates in En-DMRG runs, one needs to address the ability for En-DMRG to capture the statistics of the system for different physical quantities in comparison with ED results[66]. We will demonstrate the success of En-DMRG in this aspect as we present new results below.

To demonstrate the overall accuracy of the En-DMRG, we show the evolution of the logarithms of the energy variances averaged over more than 1000 disorder configurations as a function of the maximum bond dimension m in Fig. 2a. These results indicate the excellent convergence of the En-DMRG as we go deeper into the MBL phase ($h = 6$ and 8). For all En-DMRG results we show in this work, we keep a varying maximum bond dimension $M = 48 - 120$ states for converged and reliable results (we increase bond dimension when En-DMRG picks up a larger entropy eigenstate). The difference between En-DMRG with and without proper optimization is illustrated in Fig. 2b and Fig. 2c for the wavefunction overlap O and the local spin-z expectation value $< S^z_{N/2} >$ for the middle site of the spin chain. Without proper optimization, we find that the overlap O and $< S^z_{N/2} >$ obtained at each En-DMRG sweep is jumping around without a sign of convergence. By proper optimization, both the O and $< S^z_{N/2} >$ obtained by En-DMRG quickly converge similar to the ground state DMRG.

III. NUMERICAL RESULTS

A. The spin polarization and spin-flip

One of the characteristic features of the MBL phase is that there is a set of localized l-bits, which represents N locally conserved and commuting effective spins[9, 19–21, 56]. In general, these l-bits are locally dressed versions of the underlying physical degrees of freedom. To address the microscopic nature of l-bits and their evolution near the phase transition, we first examine the probability density distribution function of each spin for large systems. As shown in Fig. 3a, we plot the spin-z expectation value $\langle S^z_{N/2} \rangle = \langle \Psi | S^z_{N/2} | \Psi \rangle$ for the middle ($N/2$-th) site for the En-DMRG obtained eigenstate

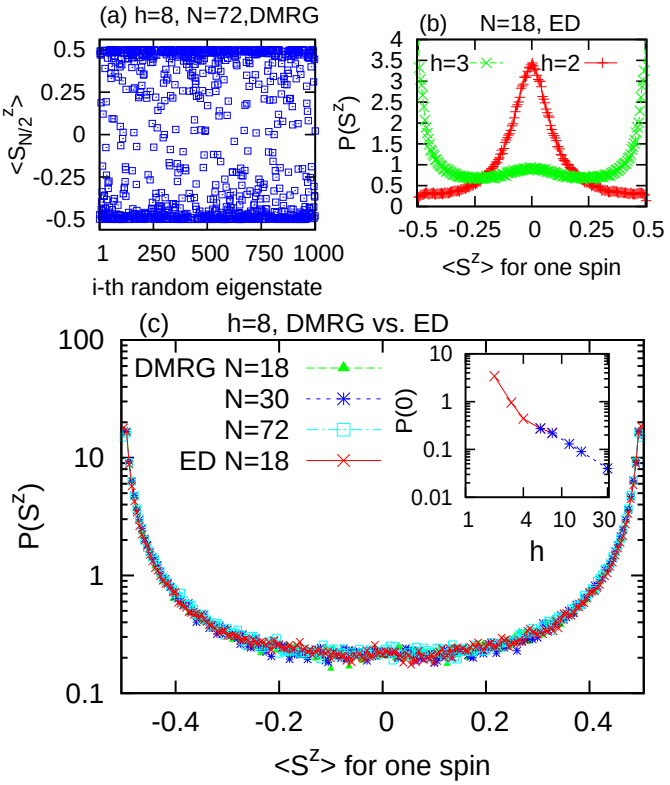

FIG. 3: (Color online) (a) The spin-z expectation values $\langle S^z_{N/2} \rangle$ for $N/2$-th site for eigenstates obtained by En-DMRG for 1000 random disorder configurations at $h = 8$ and $N = 72$. (b) The probability density distributions $P(S^z)$ for systems with weaker disorder $h = 2$ and 3 obtained by ED at $N = 18$ using an ensemble of 2000 disorder configurations with 50 states from each configuration. $P(S^z)$ has the Gaussian distribution for $h = 2$ while there are two peaks at $\langle S^z \rangle \sim \pm 0.5$ for $h = 3$. (c) $P(S^z)$ for different system sizes from $N = 18$ to $N = 72$ for strong disorder $h = 8$ using an ensemble of 20000 disorder configurations. The sharp peaks at $\langle S^z \rangle \sim \pm 0.5$ demonstrate the violation of the ETH for this system. The results obtained by En-DMRG and ED are near identical at $N = 18$ establishing the unbiased sampling for our En-DMRG. Shown in the inset is $P(0)$ as a function of h. For (b-c), the typical standard error bar (obtained by dividing ensembles into 10 groups) is about the size of the symbols.

$|\Psi\rangle$ with total $S^z_{tot} = 0$ for 1000 random disorder configurations at $N = 72$ and $h = 8$ (we take one state from each configuration). It shows a wide distribution with much enhanced appearance near $\langle S^z\rangle = \pm 0.5$ quite different from an ergodic state where the single site distribution should take on values close to the averaged value which is zero here. We have checked that spins at all other sites show very similar pattern. For comparison, we first show the probability density distribution $P(S^z)$ in Fig. 3b for systems with weak disorder $h = 2$ and 3 obtained by ED at $N = 18$ averaged over 2000 disorder configurations with 50 states near energy spectrum center from each configuration[66]. We find that $P(S^z)$ has the Gaussian distribution in the ergodic phase at $h = 2$ with a strong peak around the value $\langle S^z\rangle = 0$, which also grows sharper approaching a delta function with the increase of N. The distribution at $h = 3$ is quite different with a very broad structure and peaks near $\langle S^z\rangle \sim \pm 0.5$, which also shows a very weak N dependence.

Now we obtain the distribution function $P(S^z)$ for systems with different sizes $N = 18$, 30, and 72 in the MBL phase with $h = 8$ using 20000 disorder configurations and one state from each configuration obtained by En-DMRG as shown in Fig. 3c. We see a completely different distribution compared to the $h = 2$ result (but similar to $h = 3$ case qualitatively), with sharp peaks at $\langle S^z\rangle = \pm 0.5$ demonstrating the violation of ETH for this MBL system. The results are system size independent and fully converged suggesting the same distribution in the thermodynamic limit. By comparing the results obtained by En-DMRG and ED at $N = 18$ for $h = 8$ (in Fig. 3c) we also establish that our En-DMRG is unbiased, which reproduces all the different events with the right probability as they appear in the random quantum systems. In the $P(S^z)$ distribution function, we also see the finite probability density $P(0) \sim 0.21$ for $\langle S^z\rangle = 0$. We can understand these regions in a perturbative way. The perturbation from the xy-coupling in the Hamiltonian gives rise to spin-entangled pairs in the near polarized spin background, which we refer to as spin-flip events. The nonzero probability for $\langle S^z\rangle = 0$ is a consequence of these spin-entangled pairs. We show $P(0)$ as a function of h in the inset of Fig. 3c, which is generally nonzero for finite h approximately following $P(0) \sim 1/h$ on larger h side (we obtain results from ED in the smaller h side) revealing the significance of spin-flip events in the whole MBL phase. Because the probability density $P(0)$ is system size independent, then at large N limit, there will be a finite density for the spin-entangled pairs.

B. Distributions of entanglement entropy and fluctuation of half system magnetization

The bipartite entanglement entropy S has been extensively used as an effective tool to characterize different many-body states for such an interacting system[7, 29, 66]. We compute the Von Neumann entanglement entropy from all eigenvalues of the reduced density matrix ρ_A as $S = -\mathrm{Tr}\rho_A \ln \rho_A$, by partitioning the system in the middle of the spin chain. Different from the general volume law entanglement entropy for ergodic phase on the weak disorder side, the MBL phase at $h \gtrsim 3.5$ side has the entanglement entropy following the area law, which is the fundamental reason that DMRG can work for such a phase. We now study the probability density distribution of the entropy $P(S)$ for spin system near the energy spectrum center. We choose the statistical ensemble from at least 50000 disorder configurations for En-DMRG calculations for each N. As shown in the Fig. 4a, results from system sizes with $N = 18$, 30 and 72 are on top of each other, suggesting the same distribution in the thermodynamic limit. The agreement between the En-DMRG and ED results for $N = 18$ systems confirms the robustness of En-DMRG in capturing all different states with a wide range of the entropy distribution. The $P(S)$ results in the whole S region are converged (independent of the bond dimension) except for a couple of data points near $S \sim 0$, where the En-DMRG results are a few percent smaller than the ED results for the larger bond dimensions we used. While this small difference does not change the universal behavior of the N-independent distribution, the error is caused by the fact that these states are close to product states (which are slightly harder to be captured by En-DMRG).

Focusing on the characteristic feature of $P(S)$, we find that $P(S)$ is peaked at $S = 0$ with a continuous spectrum going into the finite S range, and with a second peak at a quantized value $S = 0.69 \sim ln2$. Quantitatively, the $P(S)$ value at the second peak is about $1/20$ of $P(S = 0)$, which is only clear in our logarithmic plot. Quite interestingly, the $P(S)$ has a smooth plateau feature on the $S < ln2$ side, but shows a large exponential drop on the $S > ln2$ side. Similar distributions are obtained for larger h, where $P(S)$ values goes to zero on the $S > ln2$ side exponentially fast with the increase of h. Comparing to the observation of the spin-flip process in the S^z distribution, we can attribute the $ln2$ peak to these small density spin-entangled pairs crossing the two half systems[51]. For strong disorder, the spin-entanglement is short-ranged and the observed $ln2$ peak has similar physical origin as the observation in the MBL phase of spinless fermion systems[28]. The continuous spectrum comes from the local interaction of spin-entangled pairs with surrounding polarized spins, which partially reduces their entanglement as they become dressed. The exponential drop of $P(S)$ on the $S > ln2$ side suggests that the events of different spin-entangled pairs getting entangled together or multi-spin resonant states have exponentially small probability for $h = 8$ deep in the MBL phase. Clearly, our method can accurately describe these rare events giving rise to large entanglement entropy.

Now we show the evolution of the $P(S)$ into the ergodic phase by reducing h. The distribution $P(S)$ for $h = 8$ to 4 are qualitatively similar as shown in Fig. 4b, with a peak at $S = 0$ and a second peak near $S = 0.69 \sim ln2$. However $P(S)$ shows much enhanced weight on the $S > ln2$ side with reducing h (results at $h = 3$ and 4 are obtained by ED), which can be fitted by a power-law behavior $P(S) \sim 1/S^x$ for $h \leq 4$. In addition, at $h = 3$, the $P(S)$ shows some different features with first peak moving away from zero to $S \sim 0.1$ and a long tail at $S > ln2$ side, which only decays

very slowly. We can still see a weak peak at $S = ln2$, which is very broad and about to disappear. Interestingly, these features for $P(S)$ at $h = 3$ is still quite different[45] from the Gaussian form with a single peak, which is the case for $h = 2$ with a sharp peak at the value $S \sim 4.7$ as we checked.

To further establish the above picture, we investigate the probability density distribution $P(F)$ of the fluctuations of the magnetization of the half system[66] defined as $F = \langle (S_h^z)^2 \rangle - \langle S_h^z \rangle^2$ calculated using the eigenstate, where S_h^z is the total spin-z component of the half system. If the half-system cutting through a spin-entangled pair while all other spins are short-range correlated (or near polarized), then we expect the variance $F = 1/4$. Interestingly, we see that the distribution $P(F)$ indeed has a second peak at the quantized value $F = 1/4$, which can be attributed to the spin-entangled pairs (local spin flips). The overall structure of $P(F)$ is very similar to $P(S)$ with the broad continuum at $F < 1/4$ side and a tail into larger F side with its magnitude growing with the reducing of h. At $h = 3$, the second peak is more robust in $P(F)$ than in $P(S)$ indicating the faster growth of the entanglement near the phase transition for finite-size systems[46].

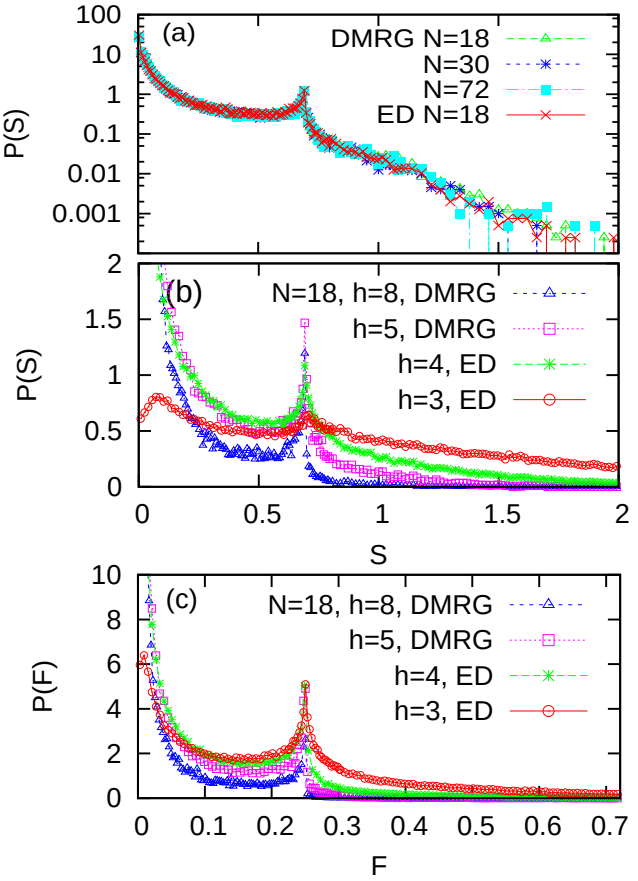

FIG. 4: (Color online) (a) The entropy probability density distribution function $P(S)$ for $N = 18$, 30 and 72 at $h = 8$. For $N = 18$, ED and En-DMRG results find excellent agreement. (b) The evolution of $P(S)$ from the MBL phase to the delocalized phase by reducing h from 8 to 3 for $N = 18$ from both ED and En-DMRG calculations. All curves have a peak at or near $S = 0$ and a second peak near $S = 0.69 \sim ln2$. $P(S)$ at larger $S > ln2$ side can be fitted by a power-law behavior $P(S) \sim 1/S^x$ for $h \leq 4$. (c) The evolution of the probability density $P(F)$ for the variance of the half system magnetization F for $h = 8, 5, 4$, and 3. The second peak is located at a quantized value $F = 1/4$. For results shown in Fig. 4, we use at least 50000 energy eigenstates for each system size. The typical standard error bar for (a-c) is about the size of symbols and it is larger near the tail of distributions.

C. Spin spin correlation function and many-body phase diagram

From the entropy distribution function we have seen that multiple spins getting entangled with each other have exponentially small probability deep inside an MBL phase, which grow with reducing h toward the transition region. Here, we seek a better understanding of this feature by calculating the disorder averaged spin-z correlations[12, 80] $C^{zz}(|i-j|) = \overline{|\langle\Psi|S_i^z S_j^z|\Psi\rangle - \langle\Psi|S_i^z|\Psi\rangle\langle\Psi|S_j^z|\Psi\rangle|}$ and spin transfer (transverse correlations) $C^{xy}(|i-j|) = \overline{|\langle\Psi|S_i^+ S_j^-|\Psi\rangle|}$ (Ψ is the excited eigenstate and the over-line represents the disorder and real space average). We find that typical spin correla-

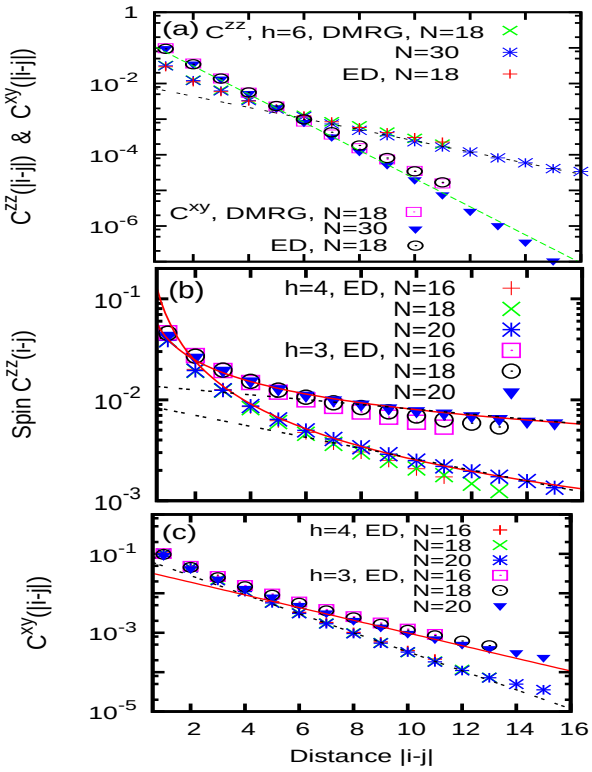

FIG. 5: (Color online) (a) The disorder averaged spin-z $C^{zz}(|i-j|)$ and spin-xy $C^{xy}(|i-j|)$ correlations obtained from En-DMRG at $h = 6$ for $N = 18$ and $N = 30$. The exponential decays can be best fit by the correlation lengths $\xi_{xy} = 1.1$ and $\xi_z = 2.78$, respectively. (b) The $C^{zz}(|i-j|)$ develops power-law correlations (see solid line fitting) for $h = 3$ and 4 obtained by ED. The dashed lines represent exponential fittings for longer distance data with $\xi_z = 18.0$ and $\xi_z = 8.0$ for $h = 3$ and 4 respectively, which show less overall agreement from the raw data comparing to the powerlaw fittings. (c) The hopping correlations $C^{xy}(|i-j|)$ decay exponentially at $h = 3$ and 4 obtained by ED. The fitting correlation lengths are $\xi_{xy} = 2.7$ and 1.8 for $h = 3$ and 4, respectively.

tions are decaying fast even for intermediate disorder strength $h \sim 4$. However, there are rare configurations where the spin correlations at larger distance are strongly enhanced, which may be related to rare Griffiths events[19, 25, 52, 80]. The arithmetic average we use here allows the rare Griffiths events to have singular contribution to the correlations near the transition region. First, we show the exponential decay behavior for these correlations in the MBL phase at $h = 6$ in Fig. 5a for $N = 18$ and 30. We find that the $C^{xy}(|i-j|)$ decays much faster than $C^{zz}(|i-j|)$ with correlation length $\xi_{xy} = 1.1$ and $\xi_z = 2.78$, respectively. Again, the ED results at $N = 18$ agree very well with the En-DMRG results.

Now we move towards the transition region by reducing h and performing ED calculations. Shown in Fig. 5b for spin-z correlations, $C^{zz}(|i-j|)$ is best fit by a power-law function $C^{zz}((i-j)) \propto 1/|i-j|^{\alpha}$ with the correlation exponents $\alpha = 0.7$ and 1.4 for $h = 3$ and 4, respectively. The fitting is more robust for larger $N = 20$ data. But due to the limited system sizes, one can also fit longer distance parts of data with exponential decay functions as illustrated by the dashed lines. The localization lengths for these fitting are $\xi_z = 8.0$ and 18.0, for $h = 4$ and 3, respecitively.

In Fig. 5c, we demonstrate the spin transverse correlations for these systems, where a clear exponential decay $C^{xy} \propto exp(-|i-j|/\xi_{xy})$ is observed with very short correlation lengths $\xi_{xy} = 2.7$ and 1.8 for $h = 3$ and 4, respectively. If we compare all correlations by fitting all data using the exponential functions as illustrated in Fig. 5(a-c), then the correlation length of the spin-z grows much faster than the one for the transverse correlations as shown in Fig. 6a with reducing h. These results clearly establish that there is an intermediate regime around $h \sim 3-4$, which has exponential decay spin transfer demonstrated from $C^{xy}(|i-j|)$, while the entanglement grows through correlations of different spin-entangled pairs seen in the power-law-like $C^{zz}(|i-j|)$ correlations. This is also consistent with the entropy distribution function, where the strong power-law tail develops on the $S > ln2$ side for these intermediate h. Based on these results, we obtain a phase diagram shown in Fig. 6b, where we find delocalized ergodic phase, a critical Griffiths regime, and an MBL phase with increasing h. From finite size results, we estimate the critical regime is between $h \sim 3.0-4.0$ based on the exponential decaying behaviors of C^{xy} before entering ergodic phase at smaller h side, and also the power-law-like behavior of the C^{zz} entering the critical Griffiths regime.

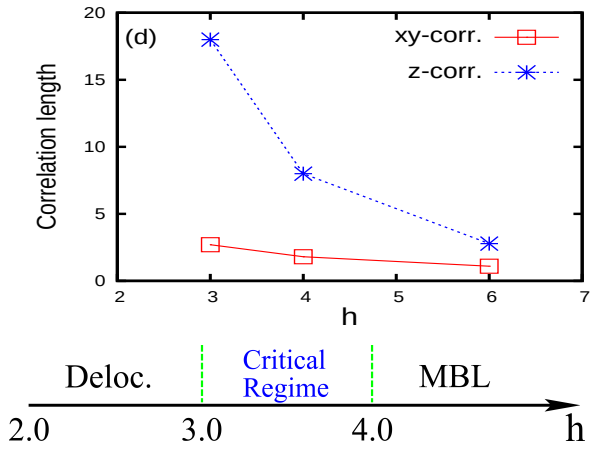

FIG. 6: (Color online) (a) For system size $N = 20$, if we fit all correlations using exponential decay functions shown in (a-c), then the correlation length for spin-z is much larger than the one for spin-xy. (b) A phase diagram with a delocalized ergodic phase, an intermediate critical Griffiths regime, and an MBL phase. See more discussions on the finite-size effect of the critical regime in the main text.

IV. SUMMARY AND DISCUSSION

Based on the newly developed En-DMRG method for excited states of MBL systems, we establish the thermodynamic distribution functions for spins, entanglement entropy and fluctuations of the half system magnetization, and demonstrate the physical picture of the MBL state. We study the dynamic phase transition from the MBL phase to the ergodic delocalized phase and find there is an intermediate Griffiths regime for disorder strength $h \sim 3-4$, where the power-law entanglement of spins develops. The intermediate critical Griffiths regime is consistent with some earlier theoretical studies using different probes[19, 24, 25, 45, 52]. Distribution functions for spin-z $P(S^z)$, entanglement entropy $P(S)$ and fluctuations of the half system magnetization $P(F)$ are all distinctly different from the ergodic phase or the MBL phase for finite-size systems, which also show slow evolution with the system size N. The basic physical picture revealed from our numerical studies is that the emergent conservation laws remain robust in the process of developing power-law entanglements in the critical Griffiths regime for systems accessible by current numerical simulations. The fate of the critical regime in the thermodynamic limit is unclear limited by the system sizes we study. However, these results may provide new insights for understanding the dynamic phase transition in such systems.

The En-DMRG algorithm we have developed is a new tool for studying outstanding and challenging issues in quantum statistical mechanics emerging in strongly interacting disorder systems. One of exciting directions is to explore the nature of MBL phase in higher dimensions as the dimensionality always plays an essential role in localization physics. Another direction is to explore the physics of the system with the quantum order including the topological order in the MBL regime. On the other hand, it is still a challenge to apply this method closer to the transition region where the entanglement distribution is extremely broad, which we hope to address in a separate work. We also hope that our results of characteristic spin correlations and distribution functions can stimulate experimental studies along this direction.

Acknowledgments - DNS thanks David Huse for stimulating discussions on DMRG for MBL states during her visit at Princeton last winter, and we also thank him for the valu-

able comments on our paper. This work is supported by US National Science Foundation Grants DMR-1408560, PREM DMR-1205734 and Princeton MRSEC Grant DMR-1420541 for travel support.

[1] D. M. Basko, I. L. Aleiner, and B. L. Altshuler, Annals of Physics **321**, 1126 (2006).
[2] L. Fleishman and P. W. Anderson, Phys. Rev. B **21**, 2366 (1980).
[3] B. L. Altshuler, Y. Gefen, A. Kamenev, and L. S. Levitov, Phys. Rev. Lett. **78**, 2803 (1997).
[4] P. Jacquod and D. L. Shepelyansky, Phys. Rev. Lett. **79**, 1837 (1997).
[5] B. Georgeot and D. L. Shepelyansky, Phys. Rev. Lett. **81**, 5129 (1998).
[6] I. V. Gornyi, A. D. Mirlin, and D. G. Polyakov, Phys. Rev. Lett. **95**, 206603 (2005).
[7] R. Nandkishore and D. A. Huse, Annu. Rev. Cond. Matt. Phys. **6**, 15 (2015).
[8] E. Altman and R. Vosk, Annu. Rev. Cond. Matt. Phys. **6**, 383 (2015).
[9] D. A. Huse, R. Nandkishore, and V. Oganesyan, Phys. Rev. B **90**, 174202 (2014).
[10] R. Nandkishore, S. Gopalakrishnan, and D. A. Huse, Phys. Rev. B **90**, 064203 (2014).
[11] V. Oganesyan and D. A. Huse, Phys. Rev. B **75**, 155111 (2007).
[12] A. Pal and D. A. Huse, Phys. Rev. B **82**, 174411 (2010).
[13] M. Žnidarič, T. Prosen, and P. Prelovšek, Phys. Rev. B **77**, 064426 (2008).
[14] M. Rigol, V. Dunjko, and M. Olshanii, Nature (London) **452**, 854 (2008).
[15] M. Serbyn, M. Knap, S. Gopalakrishnan, Z. Papić, N. Y. Yao, C. R. Laumann, D. A. Abanin, M. D. Lukin, and E. A. Demler, Phys. Rev. Lett. **113**, 147204 (2014).
[16] M. P. Kwasigroch and N. R. Cooper, Phys. Rev. A **90**, 021605 (2014).
[17] N. Y. Yao, C. R. Laumann, S. Gopalakrishnan, M. Knap, M. Müller, E. A. Demler, and M. D. Lukin, Phys. Rev. Lett. **113**, 243002 (2014).
[18] R. Vasseur, S. A. Parameswaran, and J. E. Moore, Phys. Rev. B **91**, 140202 (2015).
[19] R. Vosk, D. A. Huse, and E. Altman, ArXiv e-prints (2014), 1412.3117.
[20] M. Serbyn, Z. Papić, and D. A. Abanin, Phys. Rev. Lett. **111**, 127201 (2013).
[21] V. Ros, M. Müller, and A. Scardicchio, Nucl. Phys. B **891**, 420 (2015).
[22] A. Chandran, V. Khemani, C. R. Laumann, and S. L. Sondhi, Phys. Rev. B **89**, 144201 (2014).
[23] T. Grover, ArXiv e-prints (2014), 1405.1471.
[24] K. Agarwal, S. Gopalakrishnan, M. Knap, M. Müller, and E. Demler, Physical Review Letters **114**, 160401 (2015), 1408.3413.
[25] S. Gopalakrishnan, M. Mueller, V. Khemani, M. Knap, E. Demler, and D. A. Huse, ArXiv e-prints (2015), 1502.07712.
[26] E. Canovi, D. Rossini, R. Fazio, G. E. Santoro, and A. Silva, Phys. Rev. B **83**, 094431 (2011).
[27] E. Cuevas, M. Feigel'Man, L. Ioffe, and M. Mezard, Nat. Commun. **3**, 1128 (2012).
[28] B. Bauer and C. Nayak, J. Stat. Mech. Theor. Exp. **9**, 09005 (2013).
[29] J. A. Kjäll, J. H. Bardarson, and F. Pollmann, Phys. Rev. Lett. **113**, 107204 (2014).
[30] A. De Luca and A. Scardicchio, EPL (Europhysics Letters) **101**, 37003 (2013).
[31] S. Iyer, V. Oganesyan, G. Refael, and D. A. Huse, Phys. Rev. B **87**, 134202 (2013).
[32] D. Pekker, G. Refael, E. Altman, E. Demler, and V. Oganesyan, Phys. Rev. X **4**, 011052 (2014).
[33] S. Johri, R. Nandkishore, and R. N. Bhatt, ArXiv e-prints (2014), 1405.5515.
[34] J. H. Bardarson, F. Pollmann, and J. E. Moore, Phys. Rev. Lett. **109**, 017202 (2012).
[35] F. Andraschko, T. Enss, and J. Sirker, Phys. Rev. Lett. **113**, 217201 (2014).
[36] C. R. Laumann, A. Pal, and A. Scardicchio, Phys. Rev. Lett. **113**, 200405 (2014).
[37] J. M. Hickey, S. Genway, and J. P. Garrahan, ArXiv e-prints (2014), 1405.5780.
[38] A. Nanduri, H. Kim, and D. A. Huse, Phys. Rev. B **90**, 064201 (2014).
[39] Y. Bar Lev and D. R. Reichman, Phys. Rev. B **89**, 220201 (2014).
[40] J. Z. Imbrie, Jour. Stat. Phys. **163**, 998 (2016).
[41] T. Grover and M. P. A. Fisher, J. Stat. Mech. Theor. Exp. **10**, 10010 (2014).
[42] P. Ponte, Z. Papić, F. Huveneers, and D. A. Abanin, Phys. Rev. Lett. **114**, 140401 (2015).
[43] Y. Huang, ArXiv e-prints (2015), 1507.01304.
[44] Y.-Z. You, X.-L. Qi, and C. Xu, ArXiv e-prints (2015), 1508.03635.
[45] M. Serbyn and J. E. Moore, ArXiv e-prints (2015), 1508.07293.
[46] R. Singh, J. H. Bardarson, and F. Pollmann, ArXiv e-prints (2015), 1508.05045.
[47] Y. Bar Lev and D. R. Reichman, ArXiv e-prints (2015), 1508.05391.
[48] D.-L. Deng, J. H. Pixley, X. Li, and S. Das Sarma, ArXiv e-prints (2015), 1508.01270.
[49] X. Chen, X. Yu, G. Y. Cho, B. K. Clark, and E. Fradkin, ArXiv e-prints (2015), 1509.03890.
[50] X. Li, S. Ganeshan, J. H. Pixley, and S. Das Sarma, Phys. Rev. Lett. **115**, 186601 (2015).
[51] E. Baygan, S. P. Lim, and D. N. Sheng, Phys. Rev. B **92**, 195153 (2015).
[52] A. C. Potter, R. Vasseur, and S. A. Parameswaran, ArXiv e-prints (2015), 1501.03501.
[53] J. M. Deutsch, Phys. Rev. A **43**, 2046 (1991).
[54] M. Srednicki, Phys. Rev. E **50**, 888 (1994).
[55] P. Hosur and X.-L. Qi, ArXiv e-prints (2015), 1507.04003.
[56] A. Chandran, J. Carrasquilla, I. H. Kim, D. A. Abanin, and G. Vidal, Phys. Rev. B **92**, 024201 (2015).
[57] D. A. Huse, R. Nandkishore, V. Oganesyan, A. Pal, and S. L. Sondhi, Phys. Rev. B **88**, 014206 (2013).
[58] Y. Bahri, R. Vosk, E. Altman, and A. Vishwanath, ArXiv e-prints (2013).
[59] R. Vosk and E. Altman, Phys. Rev. Lett. **112**, 217204 (2014).
[60] A. C. Potter and A. Vishwanath, ArXiv e-prints (2015), 1506.00592.
[61] N. Y. Yao, C. R. Laumann, and A. Vishwanath, ArXiv e-prints (2015), 1508.06995.
[62] M. Schreiber, S. S. Hodgman, P. Bordia, H. P. Lüschen, M. H. Fischer, R. Vosk, E. Altman, U. Schneider, and I. Bloch, Science **349**, 842 (2015), 1501.05661.
[63] J. Smith, A. Lee, P. Richerme, B. Neyenhuis, P. W. Hess,

P. Hauke, M. Heyl, D. A. Huse, and C. Monroe, ArXiv e-prints (2015), 1508.07026.
[64] P. Bordia, H. P. Lüschen, S. S. Hodgman, M. Schreiber, I. Bloch, and U. Schneider, Physical Review Letters **116**, 140401 (2016).
[65] D. Pekker and B. K. Clark, ArXiv e-prints (2014), 1410.2224.
[66] D. J. Luitz, N. Laflorencie, and F. Alet, Phys. Rev. B **91**, 081103 (2015).
[67] J. Goold, C. Gogolin, S. R. Clark, J. Eisert, A. Scardicchio, and A. Silva, ArXiv e-prints (2015), 1504.06872.
[68] T. Devakul and R. R. P. Singh, ArXiv e-prints (2015), 1508.04813.
[69] R. Steinigeweg, J. Herbrych, F. Pollmann, and W. Brenig, ArXiv e-prints (2015), 1512.08519.
[70] O. S. Barišić, J. Kokalj, I. Balog, and P. Prelovšek, ArXiv e-prints (2016), 1603.01526.
[71] A. Chandran, C. R. Laumann, and V. Oganesyan, ArXiv e-prints (2015), 1509.04285.
[72] S. R. White, Phys. Rev. Lett. **69**, 2863 (1992).
[73] M. Friesdorf, A. H. Werner, W. Brown, V. B. Scholz, and J. Eisert, Phys. Rev. Lett. **114**, 170505 (2015).
[74] F. Pollmann, V. Khemani, J. I. Cirac, and S. L. Sondhi, ArXiv e-prints (2015), 1506.07179.
[75] A. Chandran, I. H. Kim, G. Vidal, and D. A. Abanin, Phys. Rev. B **91**, 085425 (2015).
[76] V. Khemani, F. Pollmann, and S. L. Sondhi, ArXiv e-prints (2015), 1509.00483.
[77] X. Yu, D. Pekker, and B. K. Clark, ArXiv e-prints (2015), 1509.01244.
[78] D. M. Kennes and C. Karrasch, ArXiv e-prints (2015), 1511.02205.
[79] H.-C. Jiang, Z. Wang, and L. Balents, Nature Physics **8**, 902 (2012), 1205.4289.
[80] O. Motrunich, S.-C. Mau, D. A. Huse, and D. S. Fisher, Phys. Rev. B **61**, 1160 (2000).